

Search for Lepton Number and Flavor Violation in K^+ and π^0 Decays

R. Aliberti *et al.*^{*}
(NA62 Collaboration)



(Received 17 May 2021; accepted 22 July 2021; published 24 September 2021)

Searches for the lepton number violating $K^+ \rightarrow \pi^- \mu^+ e^+$ decay and the lepton flavor violating $K^+ \rightarrow \pi^+ \mu^- e^+$ and $\pi^0 \rightarrow \mu^- e^+$ decays are reported using data collected by the NA62 experiment at CERN in 2017–2018. No evidence for these decays is found and upper limits of the branching ratios are obtained at 90% confidence level: $\mathcal{B}(K^+ \rightarrow \pi^- \mu^+ e^+) < 4.2 \times 10^{-11}$, $\mathcal{B}(K^+ \rightarrow \pi^+ \mu^- e^+) < 6.6 \times 10^{-11}$ and $\mathcal{B}(\pi^0 \rightarrow \mu^- e^+) < 3.2 \times 10^{-10}$. These results improve by 1 order of magnitude over previous results for these decay modes.

DOI: 10.1103/PhysRevLett.127.131802

Introduction.—Discovery of lepton number (LN) or lepton flavor number (LF) violation would be a clear indication of new physics; although they are conserved quantum numbers in the standard model (SM), their conservation is not imposed by any local gauge symmetry. Observation of neutrino oscillations provided the first proof of the nonconservation of LF, however no evidence of LN violation has been observed so far. New physics models which explain experimental observations, such as neutrino oscillations or the possible flavor anomalies in B physics [1], can introduce LN and LF violation. The seesaw mechanism [2] provides a source of LN violation through the exchange of Majorana neutrinos, as in neutrinoless double beta decay. Processes violating LF conservation can occur via the exchange of leptoquarks [3,4], of a Z' boson [5,6] or in SM extensions with light pseudoscalar bosons [7]. Searches for kaon decays violating LN and LF conservation are powerful probes of models beyond the SM at mass scales up to $\mathcal{O}(100 \text{ TeV})$. These complement searches in B meson or lepton decays, such as those producing recent limits on branching ratios $\mathcal{B}(B^+ \rightarrow K^+ \mu^- e^+) < 7.0 \times 10^{-9}$ [8] and $\mathcal{B}(\mu^+ \rightarrow e^+ \gamma) < 4.2 \times 10^{-13}$ [9], which explore different aspects of new physics models. An indirect upper limit on $\mathcal{B}(K^+ \rightarrow \pi^- \mu^+ e^+)$ of a few units $\times 10^{-11}$ has been derived from an upper limit on the $\mu^- + (Z, A) \rightarrow e^+ + (Z - 2, A)$ conversion probability [10]. Previous experimental limits on LN and LF violating K^+ and π^0 decays are reported in Table I.

In this Letter searches are presented for the LN violating $K^+ \rightarrow \pi^- \mu^+ e^+$ decay (π^- channel), and the LF violating

decays $K^+ \rightarrow \pi^+ \mu^- e^+$ (μ^- channel) and $\pi^0 \rightarrow \mu^- e^+$, using the data collected by the NA62 experiment at the CERN SPS in 2017–2018.

Beam line and detector.—A sketch of the NA62 beam line and detector is shown in Fig. 1 and a detailed description can be found in Ref. [16]. Kaons are produced in the interaction of a high intensity 400 GeV proton beam extracted from the CERN SPS with a beryllium target. The resulting secondary hadron beam of positively charged particles consists of 70% π^+ , 23% protons, and 6% K^+ , with a nominal momentum of 75 GeV/c (1% rms momentum bite). Beam kaons are identified by a differential Cherenkov counter (KTAG) with 70 ps time resolution and reconstructed using a silicon pixel beam spectrometer (GTK). The momenta and directions of charged particles produced in K^+ decays in a 75 m long fiducial volume (FV) are measured by a magnetic spectrometer (STRAW). Particle identification is provided by a ring-imaging Cherenkov detector (RICH), a quasihomogeneous liquid krypton electromagnetic calorimeter (LKr), hadronic calorimeters (MUV1,2), and a muon detector (MUV3). A photon veto system includes the LKr, twelve ring-shaped

TABLE I. Summary of previous experimental limits at 90% C.L. on the branching ratios of LN and LF violating K^+ and π^0 decays.

	Limit at 90% C.L.
$K^+ \rightarrow \pi^- \mu^+ \mu^+$	$< 4.2 \times 10^{-11}$ (NA62 at CERN [11])
$K^+ \rightarrow \pi^- e^+ e^+$	$< 2.2 \times 10^{-10}$ (NA62 at CERN [11])
$K^+ \rightarrow \pi^- \mu^+ e^+$	$< 5.0 \times 10^{-10}$ (E865 at BNL [12])
$K^+ \rightarrow \pi^+ \mu^- e^+$	$< 5.2 \times 10^{-10}$ (E865 at BNL [12])
$K^+ \rightarrow \pi^+ \mu^+ e^-$	$< 1.3 \times 10^{-11}$ (E865 at BNL [13])
$\pi^0 \rightarrow \mu^- e^+$	$< 3.4 \times 10^{-9}$ (E865 at BNL [12])
$\pi^0 \rightarrow \mu^+ e^-$	$< 3.8 \times 10^{-10}$ (E865 at BNL [14])
$\pi^0 \rightarrow \mu^\pm e^\mp$	$< 3.6 \times 10^{-10}$ (KTeV at FNAL [15])

*Full author list given at the end of the Letter.

Published by the American Physical Society under the terms of the Creative Commons Attribution 4.0 International license. Further distribution of this work must maintain attribution to the author(s) and the published article's title, journal citation, and DOI. Funded by SCOAP³.

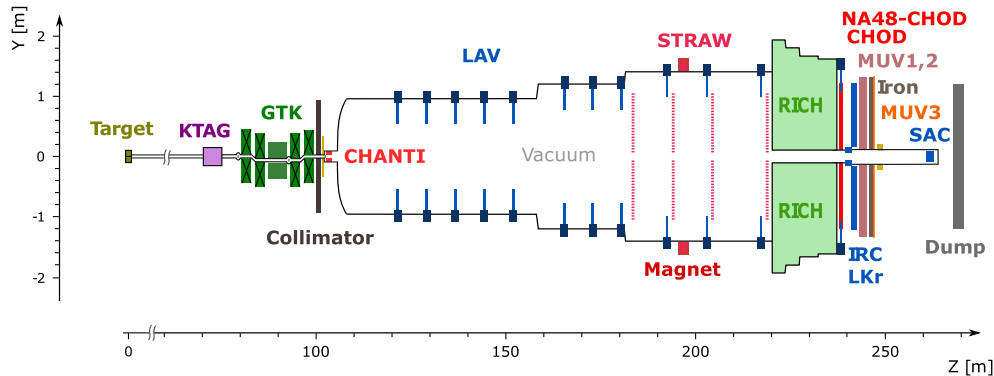


FIG. 1. Schematic side view of the NA62 beam line and detector. Information from the CHANTI, IRC, and SAC veto detectors, MUV1,2 hadronic calorimeters, and GTK beam spectrometer is not used in this analysis.

lead-glass detectors (LAV1–12) and small angle calorimeters (IRC and SAC). The RICH provides a trigger time with 70 ps precision. Two scintillator hodoscopes, NA48-CHOD and CHOD, each arranged in four quadrants, provide trigger signals and time measurements for charged particles with 200 and 800 ps precision, respectively.

Data sample and trigger.—The data sample consists of 8.3×10^5 SPS spills collected in 2017 and 2018 with a typical primary beam intensity of 2.2×10^{12} protons per spill of three seconds effective duration, corresponding to a mean K^+ decay rate in the FV of 3.7 MHz. The trigger system is composed of a hardware level (L0) and a software level (L1), with maximum output rates of 1 MHz and 10 kHz, respectively [17]. The three trigger chains used for this analysis run concurrently with the trigger chain dedicated to the main goal of the experiment, the measurement of the $K^+ \rightarrow \pi^+ \nu \bar{\nu}$ branching ratio [18]: the multitrack (MT), electron multitrack (*e*MT), and muon multitrack (μ MT) triggers.

The MT L0 trigger requires a signal in the RICH, and a time coincidence of signals in two opposite CHOD quadrants. The *e*MT trigger collects a sample enriched with electrons, which deposit almost all of their energy in the LKr, by additionally requiring a minimum energy deposit of 20 GeV in the LKr (LKr20 signal). The μ MT trigger selects at least one muon in the final state, requiring in addition to the MT conditions a coincident signal in the MUV3 and a minimum energy deposit of 10 GeV in the LKr (LKr10 signal). The common L1 trigger conditions select events with a K^+ identified by the KTAG within 5 ns of the trigger time, and a track of a negatively charged particle reconstructed in the STRAW. For most of the data sample the L1 μ MT trigger also requires fewer than 3 signals in total in LAV stations 2–11 within 6 ns of the trigger time. The MT, μ MT, and *e*MT trigger chains are downsampled typically by factors $D_{\text{MT}} = 100$, $D_{\mu\text{MT}} = 8$, and $D_{e\text{MT}} = 8$, respectively, but these values were varied during data taking.

Data collected with a minimum bias trigger, requiring the presence of a signal in the NA48-CHOD at L0 and

downscaled by a factor of 400, are used for particle identification and trigger efficiency studies.

Analysis strategy and event selection.—The branching ratios for signal decays are measured relative to the normalization channel $K^+ \rightarrow \pi^+ \pi^+ \pi^-$ ($K_{3\pi}$) which, because of a similar topology to the signal decays, allows a first order cancellation of systematic effects related to trigger conditions and detector inefficiencies.

The MT, *e*MT, and μ MT trigger chains are used to collect signal events, and the MT trigger chain is used to collect normalization events.

Acceptances for the signal and normalization channels are evaluated using Monte Carlo (MC) detector simulations based on the GEANT4 toolkit [19].

The event selection identifies events comprising three tracks which point to the active region of the downstream detectors used in the analysis, are within 5 ns of the trigger time, and form a vertex of total charge +1 with a longitudinal distance from the target $105 < Z_{vtx} < 180$ m. A vertex time is defined as the weighted mean of the track times, with weights assigned based on the time resolution of the detector (CHOD or NA48-CHOD) used to define the track time. To confirm that the beam particle is a K^+ , a KTAG signal must be present within 3 ns of the vertex time. Events with LAV signals within 3 ns of the trigger time are rejected, providing a photon veto. The total three-momentum at the vertex must have a magnitude consistent with the measured mean K^+ beam momentum within 2.5 GeV/c and its transverse component with respect to the beam axis is required to be less than 35 MeV/c , to reject events with missing energy.

For the normalization channel selection, the three-track invariant mass reconstructed under the 3π mass hypothesis is required to be consistent with the charged kaon mass within $3\sigma_{3\pi}$, where the measured mass resolution is $\sigma_{3\pi} = 0.9 \text{ MeV}/c^2$.

Signal selection requires particle identification (PID) conditions using information from the LKr and MUV3 detectors to isolate candidate $\pi^\mp \mu^\pm e^\pm$ final states. For each

track the ratio, E/p , is calculated from the energy (E) of the associated LKr cluster and its momentum (p). If no signal in MUV3 is associated with the track, a pion is identified if $E/p < 0.9$ while a positron is identified if $0.95 < E/p < 1.05$. For a positron, exactly one associated LKr cluster must be found. A muon is identified if a MUV3 signal is associated with the track and $E/p < 0.2$. The range of the vertex longitudinal position is optimized to reduce the background from K^+ decays upstream of the FV. It is required that $Z_{vtx} > 107(111)$ m for the $\pi^- (\mu^-)$ channel.

For the π^- channel selection, the mass of the π^-e^+ pair calculated under the e^-e^+ mass hypothesis is required to exceed $140 \text{ MeV}/c^2$. This condition rejects backgrounds from $K^+ \rightarrow \pi^+\pi^0$ and $K^+ \rightarrow \pi^0\ell^+\nu_\ell$ ($\ell = \mu, e$) decays followed by $\pi^0 \rightarrow e^+e^-\gamma$, with an e^- misidentified as a π^- .

The kinematic variable used to distinguish between signal and background is the invariant mass of the three charged tracks, $m_{\pi\mu e}$, computed by assigning the π, μ, e mass hypotheses to the tracks with corresponding identities defined by the PID requirements. The $m_{\pi\mu e}$ region close to the charged kaon mass, m_K [20], $478\text{--}510 \text{ MeV}/c^2$ is kept masked to avoid bias in the selection optimization. This includes the signal region, $490\text{--}498 \text{ MeV}/c^2$, and $12 \text{ MeV}/c^2$ wide control regions immediately below and above the signal region (denoted CR1 and CR2, respectively), used at the final stage of the analysis to validate the background prediction. The $m_{\pi\mu e}$ resolution, obtained from simulation, is $1.4 \text{ MeV}/c^2$.

The search for the decay chain $K^+ \rightarrow \pi^+\pi^0$ followed by $\pi^0 \rightarrow \mu^-e^+$, is performed on the sample of events passing the μ^- channel selection by requiring that the reconstructed mass of the μe pair is consistent with the π^0 mass, $|m_{\mu e} - m_{\pi^0}| < 2 \text{ MeV}/c^2$. The $m_{\mu e}$ resolution obtained from simulation is $0.4 \text{ MeV}/c^2$.

Trigger efficiency.—The trigger efficiency is measured with minimum bias data. For the abundant normalization $K_{3\pi}$ events the efficiency is measured directly. On the other hand, for the signal an enriched signal-like sample is used which is selected by loosening requirements on Z_{vtx} and requiring that $m_{\pi\mu e}$ is outside the masked region. The measured efficiency of the MT trigger for normalization events is $\epsilon_n = (93.2 \pm 0.5) \times 10^{-2}$, and the result for signal-like events is consistent with ϵ_n within 1%. The main source of MT trigger inefficiency is the STRAW condition at L1, and the uncertainty accounts for variations in the measured efficiency over time.

The L0 MUV3 and L1 LAV conditions in the μ MT trigger have negligible inefficiency for signal-like events since similar conditions are applied offline in the selection. The efficiencies of the LKr10 and LKr20 conditions present in the μ MT and e MT triggers, respectively, depend on the total energy deposited in the LKr. The energy deposited by the pion in the LKr is not precisely reproduced

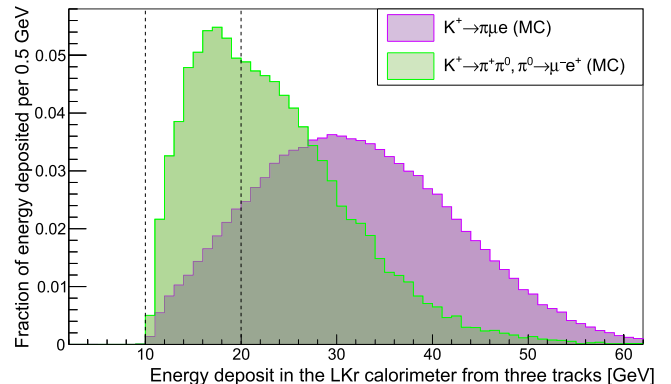


FIG. 2. Distributions of energy deposited in the LKr associated with the three selected STRAW tracks for events passing the signal selection, $K^+ \rightarrow \pi^\pm \mu^\mp e^\pm$ and $K^+ \rightarrow \pi^+\pi^0$ followed by $\pi^0 \rightarrow \mu^-e^+$, obtained from MC simulations after data-driven corrections to the energy of the LKr pion cluster.

in simulations, so a correction to this quantity is applied based on measurements. After this correction, energy-dependent trigger inefficiencies are applied in the simulation. The softer electron spectrum for $K^+ \rightarrow \pi^+\pi^0$ followed by $\pi^0 \rightarrow \mu^-e^+$ decays, with respect to $K^+ \rightarrow \pi^\pm \mu^\mp e^\pm$ (Fig. 2), leads to a lower efficiency of the LKr10 and LKr20 trigger conditions, as will be shown below.

Normalization to $K_{3\pi}$ decay.—The effective number of K^+ decays in the FV is

$$N_K = \sum_i N_K^i = \frac{1}{\mathcal{B}(K_{3\pi}) A_n \epsilon_n} \cdot \sum_i \left(N_{3\pi}^i \frac{D_{\text{MT}}^i}{D_{\text{eff}}^i} \right) = (1.33 \pm 0.02) \times 10^{12}, \quad (1)$$

where the index i runs over data-taking periods defined by constant trigger downscaling factors, $N_{3\pi}^i$ are the numbers of normalization $K_{3\pi}$ events selected with the MT trigger with downscaling factor D_{MT}^i , and D_{eff}^i are the effective downscaling factors of the three signal trigger chains. These are evaluated as

$$D_{\text{eff}}^i = \left[1 - \left(1 - \frac{1}{D_{\text{MT}}^i} \right) \left(1 - \frac{1}{D_{\mu\text{MT}}^i} \right) \left(1 - \frac{1}{D_{e\text{MT}}^i} \right) \right]^{-1} \quad (2)$$

and vary in the range 3.2–6.9. In Eq. (1), $\mathcal{B}(K_{3\pi}) = (5.583 \pm 0.024) \times 10^{-2}$ [20] and $A_n = 10.18 \times 10^{-2}$ are the branching ratio and selection acceptance (determined using simulation) of the $K_{3\pi}$ decay, and ϵ_n is the efficiency of the MT trigger for the normalization channel. The total number of selected $K_{3\pi}$ events collected with the MT trigger is $\sum_i N_{3\pi}^i = 2.73 \times 10^8$. The quoted uncertainty in N_K accounts for any inaccuracy in the description of the beam momentum spectrum and STRAW inefficiency in simulations.

Backgrounds.—Backgrounds arise from K^+ decays followed by particle misidentification and $\pi^\pm \rightarrow \ell^\pm \nu_\ell$ ($\ell = \mu, e$) decays in flight. The probability of at least one π^\pm , from a $K_{3\pi}$ decay in the FV, to decay upstream of the LKr is found using simulations to be 7.5%, with the ratio of decay rates $\Gamma(\pi^\pm \rightarrow e^\pm \nu_e) / \Gamma(\pi^\pm \rightarrow \mu^\pm \nu_\mu) = 1.23 \times 10^{-4}$ [20].

Particle misidentification.—Misidentification of $\pi^\pm \rightleftharpoons e^\pm$ arises from E/p measurements. The misidentification probabilities are measured using samples of $K_{3\pi}$ ($\pi^\pm \rightarrow e^\pm$) and $K^+ \rightarrow \pi^+ \pi^0$ followed by $\pi^0 \rightarrow e^+ e^- \gamma$ ($e^\pm \rightarrow \pi^\pm$) decays, collected with the minimum bias trigger. In each sample, the measured contamination from other K^+ decays is below 10^{-4} . The misidentification probabilities are momentum dependent with values $P(\pi^\pm \rightarrow e^\pm) = (4 - 5) \times 10^{-3}$ and $P(e^\pm \rightarrow \pi^\pm) = (1 - 3) \times 10^{-2}$.

Misidentification of π^\pm as μ^\pm arises from accidental matching of tracks with MUV3 signals or pion-induced showers in hadron calorimeters producing muons. Accidental MUV3 signals are simulated using rates measured in time sidebands within 45–75 ns of the trigger time, and hadronic showers are simulated using GEANT4. The misidentification probability is position and momentum dependent, with values of $P(\pi^\pm \rightarrow \mu^\pm) = (2-3) \times 10^{-3}$.

Misidentification of μ^\pm as π^\pm occurs due to inefficiency of the MUV3 detector. This inefficiency is measured to be 1.5×10^{-3} using kinematically selected $K^+ \rightarrow \mu^+ \nu_\mu$ decays from minimum-bias data, and beam halo muons.

The misidentification of e^\pm as μ^\pm , with probability $P(e^\pm \rightarrow \mu^\pm) = \mathcal{O}(10^{-8})$, occurs when an e^\pm is absorbed or scattered inelastically upstream of the LKr. In this case no LKr energy deposit is recorded, and the track is matched with an accidental signal in MUV3. The misidentification probability is measured from data using a sample of MUV3 signals in time sidebands and depends on track momentum and extrapolated track position at MUV3.

Background evaluation.—Simulations that include data-driven corrections are used to predict the background. Each simulated event is assigned a weight, which accounts for misidentification probabilities and corrects for discrepancies between data and simulations in energy deposited by π^\pm in the LKr, as well as in the beam momentum spectrum.

The number of selected data events with $m_{\pi\mu e} < 478 \text{ MeV}/c^2$ agree with predictions from simulations within 3% for both the π^- and μ^- channels (Fig. 3). The composition of backgrounds is similar in the control regions (CR1 and CR2) and in the signal regions. After unmasking the control regions, the predicted and observed numbers of events are largely consistent (Table II). The predicted numbers of background events from each source in the signal regions are given in Table III. The main contributions to the quoted uncertainties are the limited statistics of the simulations and the accuracy of the misidentification models.

Single event sensitivity.—The single event sensitivities, $\mathcal{B}_{\text{SES}}^i$, defined for each process as the branching ratio

TABLE II. Predicted backgrounds and observed numbers of events in control regions CR1 and CR2.

	$K^+ \rightarrow \pi^- \mu^+ e^+$		$K^+ \rightarrow \pi^+ \mu^- e^+$	
	CR1	CR2	CR1	CR2
Predicted	1.68 ± 0.20	1.66 ± 0.26	3.41 ± 0.54	1.27 ± 0.40
Observed	2	4	2	0

corresponding to the observation of one signal event, are computed for each data-taking period, i , as

$$\mathcal{B}_{\text{SES}}^i = \frac{1}{N_K^i A_s \epsilon_s^i} = \mathcal{B}(K_{3\pi}) \frac{A_n D_{\text{eff}}^i}{A_s N_{3\pi}^i D_{\text{MT}}^i} \frac{\epsilon_n}{\epsilon_s^i}, \quad (3)$$

where A_s are the signal acceptances (computed using simulations assuming uniform phase-space density), and ϵ_s^i are the trigger efficiencies for signal events, which vary due to changes in trigger downscaling factors. Efficiencies for trigger components present in both normalization and signal trigger chains cancel in Eq. (3) to 1% precision, except for the LKr10(20) components ($\epsilon_{\text{LKr10(20)}}$), which depend on the energy deposited in the LKr and are not present in the MT trigger chain. Therefore,

$$\frac{\epsilon_s^i}{\epsilon_n} = \left[1 - \left(1 - \frac{1}{D_{\text{MT}}^i} \right) \left(1 - \frac{\epsilon_{\text{LKr10}}}{D_{\mu\text{MT}}^i} \right) \left(1 - \frac{\epsilon_{\text{LKr20}}}{D_{e\text{MT}}^i} \right) \right] D_{\text{eff}}^i. \quad (4)$$

A summary of inputs to the single event sensitivity calculation is given in Table IV. For the $\pi^0 \rightarrow \mu^- e^+$ search, $\mathcal{B}_{\text{SES}}^i$ is divided by $\mathcal{B}(K^+ \rightarrow \pi^+ \pi^0) = (20.67 \pm 0.08) \times 10^{-2}$ [20].

The quantity \mathcal{B}_{SES} for the full dataset is given by

$$\mathcal{B}_{\text{SES}} = \left[\sum_i (\mathcal{B}_{\text{SES}}^i)^{-1} \right]^{-1}, \quad (5)$$

and results are shown in Table IV. The uncertainty in \mathcal{B}_{SES} includes the external error from the branching fractions

TABLE III. Predicted numbers of background events in signal regions. Decays upstream of the FV are the primary component of the $K^+ \rightarrow \pi^+ \pi^+ \pi^-$ background.

Source	$K^+ \rightarrow \pi^- \mu^+ e^+$	$K^+ \rightarrow \pi^+ \mu^- e^+$	$\pi^0 \rightarrow \mu^- e^+$
$K^+ \rightarrow \pi^+ \pi^+ \pi^-$	0.22 ± 0.15	0.84 ± 0.34	0.22 ± 0.15
$K^+ \rightarrow \pi^+ e^+ e^-$	0.63 ± 0.13	negligible	negligible
$K^+ \rightarrow \mu^+ \nu_\mu e^+ e^-$	0.13 ± 0.02	negligible	negligible
$K^+ \rightarrow \pi^+ \pi^- e^+ \nu_e$	0.07 ± 0.02	0.05 ± 0.03	0.01 ± 0.01
$K^+ \rightarrow \pi^+ \mu^+ \mu^-$	0.01 ± 0.01	0.02 ± 0.01	negligible
$K^+ \rightarrow e^+ \nu_e \mu^+ \mu^-$	0.01 ± 0.01	0.01 ± 0.01	negligible
Total	1.07 ± 0.20	0.92 ± 0.34	0.23 ± 0.15

TABLE IV. Summary of inputs to the single event sensitivity calculation and corresponding resulting values for each search. The signal acceptances, A_s , are displayed with statistical uncertainties only; other uncertainties quoted are quadratic sums of the statistical and systematic uncertainties.

	$K^+ \rightarrow \pi^- \mu^+ e^+$	$K^+ \rightarrow \pi^+ \mu^- e^+$	$\pi^0 \rightarrow \mu^- e^+$
$A_s \times 10^2$	4.90 ± 0.02	6.21 ± 0.02	3.11 ± 0.02
$\varepsilon_{\text{LKr}10} \times 10^2$	97.5 ± 1.3	97.5 ± 1.3	92.9 ± 1.2
$\varepsilon_{\text{LKr}20} \times 10^2$	74.1 ± 1.6	73.3 ± 1.6	45.3 ± 1.0
$\mathcal{B}_{\text{SES}} \times 10^{11}$	1.82 ± 0.08	1.44 ± 0.05	13.9 ± 0.9

$\mathcal{B}(K_{3\pi})$ and $\mathcal{B}(K^+ \rightarrow \pi^+ \pi^0)$, each 0.4% in relative terms, and search-specific systematic uncertainties (2%–7%) of \mathcal{B}_{SES} , assigned to account for the precision of the data-driven corrections applied in simulations. For the LF violating $K^+ \rightarrow \pi^+ \mu^+ e^-$ decay $\mathcal{B}_{\text{SES}} = (1.46 \pm 0.06) \times 10^{-11}$ and for the $\pi^0 \rightarrow \mu^- e^+$ decay $\mathcal{B}_{\text{SES}} = (15.9 \pm 1.1) \times 10^{-11}$. Neither of these sensitivities are competitive with previous searches [13,15].

Results.—After unmasking the signal regions, the mass spectra for the $K^+ \rightarrow \pi^- \mu^+ e^+$ and $K^+ \rightarrow \pi^+ \mu^- e^+$ searches are shown in Fig. 3. The numbers of predicted backgrounds (n_{bg}) and observed events (n_{obs}) in the signal regions are listed below

$$\begin{aligned} K^+ \rightarrow \pi^- \mu^+ e^+: n_{\text{bg}} &= 1.07 \pm 0.20, & n_{\text{obs}} &= 0; \\ K^+ \rightarrow \pi^+ \mu^- e^+: n_{\text{bg}} &= 0.92 \pm 0.34, & n_{\text{obs}} &= 2; \\ \pi^0 \rightarrow \mu^- e^+: n_{\text{bg}} &= 0.23 \pm 0.15, & n_{\text{obs}} &= 0. \end{aligned}$$

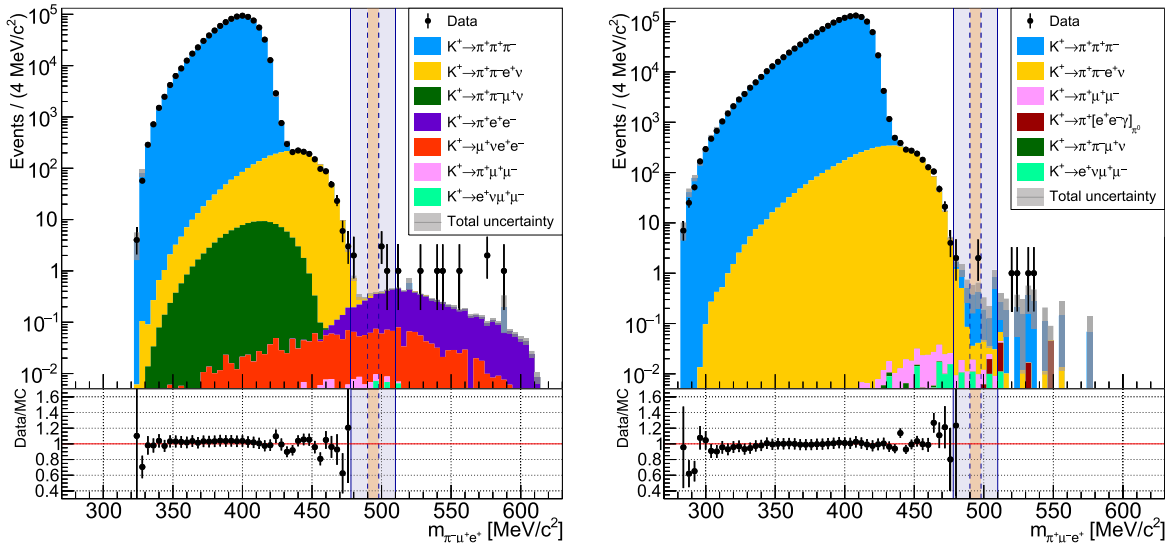


FIG. 3. Reconstructed $m_{\pi\mu e}$ spectra for selected events in searches for $K^+ \rightarrow \pi^- \mu^+ e^+$ (left) and $K^+ \rightarrow \pi^+ \mu^- e^+$ (right) for data (black markers) and simulated background (filled areas) samples. Ratios between the observed numbers of data events and the predicted numbers of events from MC simulations are shown in the lower panels.

The observations are consistent with the background predictions, and upper limits are set for the branching ratios using the C.L.s method [21] with a likelihood ratio test statistic. The upper limits obtained at 90% C.L. are

$$\begin{aligned} \mathcal{B}(K^+ \rightarrow \pi^- \mu^+ e^+) &< 4.2 \times 10^{-11}; \\ \mathcal{B}(K^+ \rightarrow \pi^+ \mu^- e^+) &< 6.6 \times 10^{-11}; \\ \mathcal{B}(\pi^0 \rightarrow \mu^- e^+) &< 3.2 \times 10^{-10}. \end{aligned}$$

Conclusions.—Searches for the LN violating $K^+ \rightarrow \pi^- \mu^+ e^+$, and LF violating $K^+ \rightarrow \pi^+ \mu^- e^+$ and $\pi^0 \rightarrow \mu^- e^+$ decays are reported. No evidence for these decays is found and upper limits are established at 90% confidence level: $\mathcal{B}(K^+ \rightarrow \pi^- \mu^+ e^+) < 4.2 \times 10^{-11}$, $\mathcal{B}(K^+ \rightarrow \pi^+ \mu^- e^+) < 6.6 \times 10^{-11}$, and $\mathcal{B}(\pi^0 \rightarrow \mu^- e^+) < 3.2 \times 10^{-10}$. These results improve on previous searches [12] by 1 order of magnitude. NA62 resumes data taking in 2021, with the primary objective of improving the precision of the study of the $K^+ \rightarrow \pi^+ \nu \bar{\nu}$ decay [18], but also with the possibility of collecting additional data to study LN and LF violating decays.

It is a pleasure to express our appreciation to the staff of the CERN laboratory and the technical staff of the participating laboratories and universities for their efforts in the operation of the experiment and data processing.

The cost of the experiment and its auxiliary systems was supported by the funding agencies of the Collaboration Institutes. We are particularly indebted to F. R. S.-FNRS (Fonds de la Recherche Scientifique—FNRS), Belgium; NSERC (Natural Sciences and Engineering Research

Council), funding SAPPJ-2018-0017 Canada; MEYS (Ministry of Education, Youth and Sports), Czech Republic; BMBF (Bundesministerium für Bildung und Forschung) Contracts No. 05H12UM5, No. 05H15UMCNA, and No. 05H18UMCNA, Germany; INFN (Istituto Nazionale di Fisica Nucleare), Italy; MIUR (Ministero dell’Istruzione, dell’Università e della Ricerca), Italy; CONACyT (Consejo Nacional de Ciencia y Tecnología), Mexico; IFA (Institute of Atomic Physics) Romanian CERN-RO No. 1/16.03.2016 and Nucleus Programme PN 19 06 01 04, Romania; INR-RAS (Institute for Nuclear Research of the Russian Academy of Sciences), Moscow, Russia; JINR (Joint Institute for Nuclear Research), Dubna, Russia; NRC (National Research Center) “Kurchatov Institute” and MESRF (Ministry of Education and Science of the Russian Federation), Russia; MESRS (Ministry of Education, Science, Research and Sport), Slovakia; CERN (European Organization for Nuclear Research), Switzerland; STFC (Science and Technology Facilities Council), United Kingdom; NSF (National Science Foundation) Grants No. 1506088 and No. 1806430, U.S.A.; ERC (European Research Council) “UniversaLepto” advanced grant 268062, “KaonLepton” starting grant 336581, Europe. Individuals have received support from Charles University Research Center (UNCE/SCI/013), Czech Republic; Ministero dell’Istruzione, dell’Università e della Ricerca (MIUR “Futuro in ricerca 2012” Grant No. RBFR12JF2Z, Project GAP), Italy; Russian Science Foundation (RSF 19-72-10096), Russia; the Royal Society (Grants No. UF100308,

No. UF0758946), United Kingdom; STFC (Rutherford fellowships ST/J00412X/1, ST/M005798/1), United Kingdom; ERC (Grants No. 268062, No. 336581 and starting Grant No. 802836 “AxScale”); EU Horizon 2020 (Marie Skłodowska-Curie Grants No. 701386, No. 754496, No. 842407, No. 893101).

- [1] R. Aaij *et al.*, arXiv:2103.11769.
- [2] P. Minkowski, Phys. Lett. **67B**, 421 (1977).
- [3] J. Pati and A. Salam, Phys. Rev. D **10**, 275 (1974).
- [4] M. Bordone *et al.*, J. High Energy Phys. 10 (2018) 148.
- [5] L. G. Landsberg, Phys. At. Nucl. **68**, 1190 (2005).
- [6] P. Langacker, Rev. Mod. Phys. **81**, 1199 (2009).
- [7] C. Cornellà, P. Paradisi, and O. Sumensari, J. High Energy Phys. 01 (2020) 158.
- [8] R. Aaij *et al.*, Phys. Rev. Lett. **123**, 241802 (2019).
- [9] A. Baldini *et al.*, Eur. Phys. J. C **76**, 434 (2016).
- [10] L. Littenberg and R. Shrock, Phys. Lett. B **491**, 285 (2000).
- [11] E. Cortina Gil *et al.*, Phys. Lett. B **797**, 134794 (2019).
- [12] R. Appel *et al.*, Phys. Rev. Lett. **85**, 2877 (2000).
- [13] A. Sher *et al.*, Phys. Rev. D **72**, 012005 (2005).
- [14] R. Appel *et al.*, Phys. Rev. Lett. **85**, 2450 (2000).
- [15] E. Abouzaid *et al.*, Phys. Rev. Lett. **100**, 131803 (2008).
- [16] E. Cortina Gil *et al.*, J. Instrum. **12**, P05025 (2017).
- [17] R. Ammendola *et al.*, Nucl. Instrum. Methods Phys. Res., Sect. A **929**, 1 (2019).
- [18] E. Cortina Gil *et al.*, J. High Energy Phys. 06 (2021) 093.
- [19] J. Allison *et al.*, Nucl. Instrum. Methods Phys. Res., Sect. A **835**, 186 (2016).
- [20] P. Zyla *et al.*, Prog. Theor. Exp. Phys. (**2020**), 083C01.
- [21] A. Read, J. Phys. G **28**, 2693 (2002).

R. Aliberti,^{5,c} F. Ambrosino,¹¹ R. Ammendola,¹⁹ B. Angelucci,³¹ A. Antonelli,¹⁰ G. Anzivino,¹² R. Arcidiacono,^{20,d}
 T. Bache,²⁹ A. Baeva,²⁴ D. Baigarashev,²⁴ M. Barbanera,¹³ J. Bernhard,²⁸ A. Biagioni,¹⁸ L. Bician,^{27,e} C. Biino,²¹
 A. Bizzeti,^{8,f} T. Blazek,²⁷ B. Bloch-Devaux,²⁰ V. Bonaiuto,^{19,g} M. Boretto,^{20,e} A. M. Bragadireanu,²³ D. Britton,³¹
 F. Brizioli,¹² M. B. Brunetti,^{29,h} D. Bryman,^{3,i} F. Bucci,⁸ T. Capussela,¹¹ J. Carmignani,³³ A. Ceccucci,²⁸ P. Cenci,¹³
 V. Cerny,²⁷ C. Cerri,¹⁶ B. Checcucci,¹³ A. Conovaloff,³⁴ P. Cooper,³⁴ E. Cortina Gil,¹ M. Corvino,^{11,e} F. Costantini,¹⁴
 A. Cotta Ramusino,⁶ D. Coward,^{34,j} G. D’Agostini,¹⁷ J. B. Dainton,³³ P. Dalpiaz,⁷ H. Danielsson,²⁸ N. De Simone,^{28,k}
 D. Di Filippo,¹¹ L. Di Lella,^{14,l} N. Doble,^{14,l} V. Duk,^{29,m} F. Duval,²⁸ B. Döbrich,²⁸ D. Emelyanov,²⁴ J. Engelfried,²² T. Enik,²⁴
 N. Estrada-Tristan,^{22,n} V. Falaleev,²⁴ R. Fantechi,¹⁶ V. Fascianelli,^{29,o} L. Federici,²⁸ S. Fedotov,²⁵ A. Filippi,²¹ M. Fiorini,⁷
 J. R. Fry,²⁹ J. Fu,³ A. Fucci,¹⁹ L. Fulton,³² E. Gamberini,²⁸ L. Gatignon,^{28,p} G. Georgiev,^{10,q} S. A. Ghinescu,²³ A. Gianoli,⁶
 M. Giorgi,¹⁴ S. Giudici,¹⁴ F. Gonnella,²⁹ E. Goudzovski,²⁹ C. Graham,³¹ R. Guida,²⁸ E. Gushchin,²⁵ F. Hahn,^{28,t} H. Heath,³⁰
 J. Henshaw,²⁹ E. B. Holzer,²⁸ T. Husek,^{4,r} O. E. Hutanu,²³ D. Hutchcroft,³² L. Iacobuzio,²⁹ E. Iacopini,⁹ E. Imbergamo,¹²
 B. Jenninger,²⁸ J. Jerhot,^{4,s} R. W. L. Jones,³³ K. Kampf,⁴ V. Kekelidze,²⁴ S. Kholodenko,²⁶ G. Khoriauli,^{5,t}
 A. Khotyantsev,²⁵ A. Kleimenova,¹ A. Korotkova,²⁴ M. Koval,^{28,u} V. Kozhuharov,^{10,q} Z. Kucerova,²⁷ Y. Kudenko,^{25,v}
 J. Kunze,⁵ V. Kurochka,²⁵ V. Kurshetsov,²⁶ G. Lamanna,¹⁴ G. Lanfranchi,¹⁰ E. Lari,¹⁴ G. Latino,⁹ P. Laycock,^{28,w}
 C. Lazzeroni,²⁹ G. Lehmann Miotto,²⁸ M. Lenti,⁹ E. Leonardi,¹⁸ P. Lichard,²⁸ L. Litov,^{24,q} R. Lollini,¹² D. Lomidze,^{5,x}
 A. Lonardo,¹⁸ P. Lubrano,¹³ M. Lupi,^{13,y} N. Lurkin,^{29,s} D. Madigozhin,²⁴ I. Mannelli,¹⁵ A. Mapelli,²⁸ F. Marchetto,²¹
 R. Marchevski,^{28,z} S. Martellotti,¹⁰ P. Massarotti,¹¹ K. Massri,²⁸ E. Maurice,^{32,aa} M. Medvedeva,²⁵ A. Mefodev,²⁵
 E. Menichetti,²⁰ E. Migliore,²⁰ E. Minucci,^{1,a,e,ab} M. Mirra,¹¹ M. Misheva,^{24,ac} N. Molokanova,²⁴ M. Moulson,¹⁰

S. Movchan,²⁴ M. Napolitano,¹¹ I. Neri,⁷ F. Newson,²⁹ A. Norton,^{7,ad} M. Noy,²⁸ T. Numao,² V. Obraztsov,²⁶ A. Ostankov,^{26,†} S. Padolski,^{1,wo} R. Page,³⁰ V. Palladino,^{28,ae} A. Parenti,⁹ C. Parkinson,^{29,s} E. Pedreschi,¹⁴ M. Pepe,¹³ M. Perrin-Terrin,^{28,af,ag} L. Peruzzo,⁵ P. Petrov,¹ Y. Petrov,² F. Petrucci,⁷ R. Piandani,^{12,ah} M. Piccini,¹³ J. Pinzino,^{28,ai} I. Polenkevich,²⁴ L. Pontisso,¹⁶ Yu. Potrebenikov,²⁴ D. Protopopescu,³¹ M. Raggi,¹⁷ A. Romano,²⁹ P. Rubin,³⁴ G. Ruggiero,^{33,z} V. Ryjov,²⁸ A. Salamon,¹⁹ C. Santoni,¹² G. Saracino,¹¹ F. Sargeni,^{19,aj} S. Schuchmann,^{28,l} V. Semenov,^{26,†} A. Sergi,^{29,ak} A. Shaikhiev,^{1,al} S. Shkarovskiy,²⁴ D. Soldi,²⁰ M. Sozzi,¹⁴ T. Spadaro,¹⁰ F. Spinella,¹⁶ A. Sturgess,²⁹ V. Sugonyaev,²⁶ J. Swallow,^{29,b} S. Trilov,³⁰ P. Valente,¹⁸ B. Velghe,² S. Venditti,²⁸ P. Vicini,¹⁸ R. Volpe,^{1,am} M. Vormstein,⁵ H. Wahl,^{7,l} R. Wanke,⁵ B. Wrona,³² O. Yushchenko,²⁶ M. Zamkovsky,⁴ and A. Zinchenko^{24,†}

(NA62 Collaboration)

*

¹*Université Catholique de Louvain, B-1348 Louvain-La-Neuve, Belgium*²*TRIUMF, Vancouver, British Columbia V6T 2A3, Canada*³*University of British Columbia, Vancouver, British Columbia V6T 1Z4, Canada*⁴*Charles University, 116 36 Prague 1, Czech Republic*⁵*Institut für Physik and PRISMA Cluster of Excellence, Universität Mainz, D-55099 Mainz, Germany*⁶*INFN, Sezione di Ferrara, I-44122 Ferrara, Italy*⁷*Dipartimento di Fisica e Scienze della Terra dell'Università e INFN, Sezione di Ferrara, I-44122 Ferrara, Italy*⁸*INFN, Sezione di Firenze, I-50019 Sesto Fiorentino, Italy*⁹*Dipartimento di Fisica e Astronomia dell'Università e INFN, Sezione di Firenze, I-50019 Sesto Fiorentino, Italy*¹⁰*Laboratori Nazionali di Frascati, I-00044 Frascati, Italy*¹¹*Dipartimento di Fisica "Ettore Pancini" e INFN, Sezione di Napoli, I-80126 Napoli, Italy*¹²*Dipartimento di Fisica e Geologia dell'Università e INFN, Sezione di Perugia, I-06100 Perugia, Italy*¹³*INFN, Sezione di Perugia, I-06100 Perugia, Italy*¹⁴*Dipartimento di Fisica dell'Università e INFN, Sezione di Pisa, I-56100 Pisa, Italy*¹⁵*Scuola Normale Superiore e INFN, Sezione di Pisa, I-56100 Pisa, Italy*¹⁶*INFN, Sezione di Pisa, I-56100 Pisa, Italy*¹⁷*Dipartimento di Fisica, Sapienza Università di Roma e INFN, Sezione di Roma I, I-00185 Roma, Italy*¹⁸*INFN, Sezione di Roma I, I-00185 Roma, Italy*¹⁹*INFN, Sezione di Roma Tor Vergata, I-00133 Roma, Italy*²⁰*Dipartimento di Fisica dell'Università e INFN, Sezione di Torino, I-10125 Torino, Italy*²¹*INFN, Sezione di Torino, I-10125 Torino, Italy*²²*Instituto de Física, Universidad Autónoma de San Luis Potosí, 78240 San Luis Potosí, Mexico*²³*Horia Hulubei National Institute of Physics for R&D in Physics and Nuclear Engineering, 077125 Bucharest-Magurele, Romania*²⁴*Joint Institute for Nuclear Research, 141980 Dubna (MO), Russia*²⁵*Institute for Nuclear Research of the Russian Academy of Sciences, 117312 Moscow, Russia*²⁶*Institute for High Energy Physics—State Research Center of Russian Federation, 142281 Protvino (MO), Russia*²⁷*Faculty of Mathematics, Physics and Informatics, Comenius University, 842 48 Bratislava, Slovakia*²⁸*CERN, European Organization for Nuclear Research, CH-1211 Geneva 23, Switzerland*²⁹*University of Birmingham, Edgbaston, Birmingham B15 2TT, United Kingdom*³⁰*University of Bristol, Bristol BS8 1TH, United Kingdom*³¹*University of Glasgow, Glasgow G12 8QQ, United Kingdom*³²*University of Liverpool, Liverpool L69 7ZE, United Kingdom*³³*University of Lancaster, Lancaster LA1 4YW, United Kingdom*³⁴*George Mason University, Fairfax, Virginia 22030, USA*[†]Deceased.^aelisa.minucci@cern.ch^bjoel.christopher.swallow@cern.ch^cPresent address: Institut für Kernphysik and Helmholtz Institute Mainz, Universität Mainz, Mainz D-55099, Germany.^dAlso at Università degli Studi del Piemonte Orientale, I-13100 Vercelli, Italy.^ePresent address: CERN, European Organization for Nuclear Research, CH-1211 Geneva 23, Switzerland.^fAlso at Dipartimento di Fisica, Università di Modena e Reggio Emilia, I-41125 Modena, Italy.^gAlso at Department of Industrial Engineering, University of Roma Tor Vergata, I-00173 Roma, Italy.^hPresent address: Department of Physics, University of Warwick, Coventry CV4 7AL, United Kingdom.ⁱAlso at TRIUMF, Vancouver, British Columbia V6T 2A3, Canada.^jAlso at SLAC National Accelerator Laboratory, Stanford University, Menlo Park, California 94025, USA.

^kPresent address: DESY, D-15738 Zeuthen, Germany.^lPresent address: Institut für Physik and PRISMA Cluster of Excellence, Universität Mainz, D-55099 Mainz, Germany.^mPresent address: INFN, Sezione di Perugia, I-06100 Perugia, Italy.ⁿAlso at Universidad de Guanajuato, 36000 Guanajuato, Mexico.^oPresent address: Center for theoretical neuroscience, Columbia University, New York, New York 10027, USA.^pPresent address: University of Lancaster, Lancaster LA1 4YW, United Kingdom.^qAlso at Faculty of Physics, University of Sofia, BG-1164 Sofia, Bulgaria.^rPresent address: Department of Astronomy and Theoretical Physics, Lund University, Lund SE 223-62, Sweden.^sPresent address: Université Catholique de Louvain, B-1348 Louvain-La-Neuve, Belgium.^tPresent address: Universität Würzburg, D-97070 Würzburg, Germany.^uPresent address: Charles University, 116 36 Prague 1, Czech Republic.^vAlso at National Research Nuclear University (MEPhI), 115409 Moscow and Moscow Institute of Physics and Technology, 141701 Moscow region, Moscow, Russia.^wPresent address: Brookhaven National Laboratory, Upton, New York 11973, USA.^xPresent address: European XFEL GmbH, D-22761 Hamburg, Germany.^yPresent address: Institut am Fachbereich Informatik und Mathematik, Goethe Universität, D-60323 Frankfurt am Main, Germany.^zPresent address: Dipartimento di Fisica e Astronomia dell'Università e INFN, Sezione di Firenze, I-50019 Sesto Fiorentino, Italy.^{aa}Present address: Laboratoire Leprince Ringuet, F-91120 Palaiseau, France.^{ab}Also at Laboratori Nazionali di Frascati, I-00044 Frascati, Italy.^{ac}Present address: Institute of Nuclear Research and Nuclear Energy of Bulgarian Academy of Science (INRNE-BAS), BG-1784 Sofia, Bulgaria.^{ad}Present address: University of Glasgow, Glasgow G12 8QQ, United Kingdom.^{ae}Present address: Physics Department, Imperial College London, London SW7 2BW, United Kingdom.^{af}Present address: Aix Marseille University, CNRS/IN2P3, CPPM, F-13288 Marseille, France.^{ag}Also at Université Catholique de Louvain, B-1348 Louvain-La-Neuve, Belgium.^{ah}Present address: University of Chinese Academy of Sciences, Beijing 100049, China.^{ai}Present address: INFN, Sezione di Pisa, I-56100 Pisa, Italy.^{aj}Also at Department of Electronic Engineering, University of Roma Tor Vergata, I-00173 Roma, Italy.^{ak}Present address: Dipartimento di Fisica dell'Università e INFN, Sezione di Genova, I-16146 Genova, Italy.^{al}Also at Institute for Nuclear Research of the Russian Academy of Sciences, 117312 Moscow, Russia.^{am}Present address: Faculty of Mathematics, Physics and Informatics, Comenius University, 842 48 Bratislava, Slovakia.